Chemical Science

EDGE ARTICLE

View Article Online
View Journal | View Issue

Cite this: *Chem. Sci.*, 2019, **10**, 4227

All publication charges for this article have been paid for by the Royal Society of Chemistry

Fluorescence lifetime imaging of upper gastrointestinal pH *in vivo* with a lanthanide based near-infrared τ probe†

Yingying Ning,[a] Shengming Cheng,[b] Jing-Xiang Wang,[a] Yi-Wei Liu,[a] Wei Feng,[b] Fuyou Li *[b] and Jun-Long Zhang *[a]

Received 15th January 2019
Accepted 23rd February 2019

DOI: 10.1039/c9sc00220k

rsc.li/chemical-science

Time-resolved fluorescence lifetime imaging (FLIM) in the near-infrared region of 900–1700 nm not only allows a deep tissue penetration depth but also offers the unique benefit of the quantitative visualization of molecular events *in vivo* and is independent of local luminescence intensity and fluorophore concentration. Herein, we report the design of a wide-range pH sensitive molecular probe based on Yb^{3+} porphyrinate. The Yb^{3+} probe shows increasing NIR emission and lifetime with pK_a values of *ca.* 6.6 from pH 9.0 and 5.0 and also displays an elongated lifetime from *ca.* 135 to 170 μs at lower pH values (5.0–1.0) due to aggregation and reduced exposure to water at low pH values. Importantly, the probe is able to monitor a wide range of *in vivo* gastrointestinal pH values in mice models and the potential applications in imaging-guided gastrointestinal diagnostics and therapeutics were revealed. This study shows that lifetime contrast is important for preclinical imaging; lanthanide complexes could be successfully used in the design of stimuli-responsive NIR τ probes for advanced *in vivo* imaging.

Introduction

Determining gastric juice acidity *in vivo* is the primary step for the accurate diagnosis and treatment of upper gastrointestinal diseases,[1–3] and helps the development of pH-triggered stomach medicines.[4,5] Traditionally, the standard clinical method to assess stomach pH values relies on invasive endoscopic tests, however these are uncomfortable for patients and are not suitable for long-term monitoring.[6] Given such limitations, several approaches have been explored to measure stomach pH *in vivo*, for instance ingestible electronic capsules such as "Heidelberg" and "Bravo" have been developed,[7] but the sizes[8] and functions[9] still need to be technically modified. Fluorescence imaging is no doubt a promising non-invasive method for upper gastrointestinal pH detection. Since 1965, organic dyes including "Congo red" have been introduced,[10,11] but endoscopy or *ex vivo* experiments are still required to assist the optical measurements due to the limited tissue penetration depth. Thus, the development of a non-invasive method that is more convenient, safer and faster for accurately assessing *in vivo* upper gastrointestinal pH is of importance.

Fluorescence imaging in the near-infrared (NIR) region of 900–1700 nm, as an advanced non-invasive technique with an enhanced penetration depth, has attracted increasing attention due to its reduced tissue absorption, autofluorescence and photon scattering.[12,13] However, quantitative monitoring of physicochemical environments such as temperature, pH and viscosity in this region still remains a challenge *in vivo*, as fluorescence intensity is dependent on concentration gradient, the heterogeneity of tissues, excitation power *etc.* In contrast to intensity, lifetime τ is an intrinsic characteristic of fluorophores and is largely independent on concentration and thus fluorescence lifetime imaging microscopy (FLIM) has recently emerged as an intrinsically quantitative technique for detecting lifetime as marker.[14,15] Therefore, exploring a lifetime-based NIR probe, in terms of an NIR τ probe, being able to report local physicochemical parameters allows the establishment of FLIM as a quantitative non-invasive approach in the NIR region.

Thanks to the recent advances in NIR imaging, there are an increasing number of NIR fluorophores available.[12,13] However, designing NIR τ probes (900–1700 nm) with pH-induced distinct lifetime changes is a synthetic challenge. Moreover, *in vivo* pH variation in the upper gastrointestinal tract is wide-ranging, for example stomach pH (1–3) and intestine pH (6–7), and most pH probes possess sensitive luminescence with a narrow p$K_a \pm 1$ range (ΔpH = 2). Furthermore, environmental responsive lifetime contrast is important for designing τ probes. NIR organic fluorophores are not preferable as τ probes due to

[a]*Beijing National Laboratory for Molecular Sciences, State Key Laboratory of Rare Earth Materials Chemistry and Applications, College of Chemistry and Molecular Engineering, Peking University, Beijing 100871, P. R. China. E-mail: zhangjunlong@pku.edu.cn*

[b]*Department of Chemistry, State Key Laboratory of Molecular Engineering of Polymers, Institutes of Biomedical Sciences, Fudan University, Shanghai 200433, P. R. China*

† Electronic supplementary information (ESI) available: Detailed synthesis and characterization data; ^{1}H and ^{19}F NMR spectra, IR spectra and MS spectra. See DOI: 10.1039/c9sc00220k

their low lifetime contrast compared with autofluorescence background. Despite the fact that quantum dots[16,17] and lanthanide-doped nanoparticles[18,19] can achieve long lifetimes, they still suffer from decomposition and unknown toxicity concerns under strong acidic environments like stomach.[20] To address these issues, we herein introduce a new strategy for constructing NIR τ probes based on lanthanide (Ln) coordination complexes by combining the features of organic molecules (small sizes and low cytotoxicity) and metal ions (metal characteristic luminescence and long decay lifetimes up to microseconds).[21–23]

The microsecond scaled lifetime of lanthanides allows for effective discrimination from the noise of autofluorescence (nanosecond scale) and thus achieves a high signal to noise ratio.[24–26] Due to the forbidden f–f transition, the emission of lanthanide complexes, especially europium(III) and terbium(III), has been extensively used for τ probes in bioanalysis and cell imaging.[27,28] In contrast to visible emissive Ln, NIR Ln has not been widely considered for τ probes,[29–32] although they have been employed as luminescent biosensors for two decades.[33–35] One possible reason is their low quantum yields,[29–32] making it difficult to collect enough photons to obtain FLIM images with good quality. Recently, we reported highly luminescent ytterbium (Yb^{3+}) porphyrinates with long lifetimes up to *ca.* 700 μs,[36] which were applicable in living cell imaging dependent on either emission intensity or lifetime.[37] This enables the Yb^{3+} complexes as a promising molecular platform for constructing NIR τ probes (900–1100 nm), but further precise modification of the porphyrin structure is required to design stimuli-responsive Yb^{3+} τ probes for *in vivo* pH detection.

To demonstrate the perspective in a preclinical study, in this work, we designed a pH-sensitive Yb^{3+} porphyrinate (**F-Yb**) as an NIR τ probe by introducing a carboxylate group to the *meso*-position of porphyrin. **F-Yb** showed increasing NIR emission as well as lifetime within a physiologically relevant pH range from 9.0 and 5.0, with a pK_a of *ca.* 6.6. Serendipitously, this NIR τ probe tends to aggregate when the pH is lower than 5.0. A decrease in solubility arising from aggregation reduces the exposure of the Yb^{3+} complex to water and elongates the lifetime (from *ca.* 135 to 170 μs), which renders **F-Yb** a low pH (5.0 to 1.0) NIR τ probe. Using oral gavage experiments in nude mice, **F-Yb** was able to detect real-time pH changes during the normal metabolic process, fasting experiments, and treatment with hydrotalcite drugs, with significant lifetime contrast and quantitative pH measurements *in vivo*. These results clearly demonstrate the effectiveness of lanthanide NIR τ probes for quantitatively visualizing local physicochemical parameters *in vivo*, with the potential for preclinical diagnostic and therapeutic studies.

Results and discussion

Synthesis and characterization

A judicious choice of *meso*-aryl group is critical for designing wide-range pH-sensitive Yb^{3+} τ probes, as β-fluorination is a prerequisite for high NIR luminescence as well as a long lifetime and thus β-periphery should be kept intact.[36] In this work, we introduced a 4-carboxyphenyl group to the *meso*-position to synthesize 2,3,7,8,12,13,17,18-octafluoro-5,10,15,20-tetra(4-carboxyphenyl)porphyrin-ytterbium(III)-L_{OCD3} (**F-Yb**, L_{OCD3} = (cyclopentadienyl)tris(di(methyl-d_3)phosphito)cobaltate). **F-Yb** was obtained in an overall yield of 58% starting from 4-methyl formylbenzoate and 3,4-difluoropyrrole (Scheme 1). As controls, **F-Yb-1**, which contains only one 4-carboxyphenyl group, and the β-periphery hydrogenated complex **H-Yb** were synthesized. To investigate the possibility of energy transfer from the ligand to Yb^{3+}, we prepared the corresponding Gd^{3+} complex **F-Gd** to estimate the energy level of the lowest triplet state of the ligand by phosphorescence, because the excited state of Gd^{3+} is high-lying compared to the lowest triplet state of porphyrinates.[38] Their structures were characterized by ^{1}H, ^{19}F-NMR, UV-vis and IR spectroscopy and high resolution ESI mass spectrometry. Detailed synthetic procedures and characterizations are presented in the Experimental section and the ESI.†

In vitro pH sensitivity (from pH 9.0–1.0)

(1) pH 9.0–5.0. F-Yb and **F-Yb-1** show similar absorption in water, in which the Soret bands are centered at *ca.* 410 nm and the Q bands cover the region of 500–650 nm with extinction coefficients larger than 10^4 M^{-1} cm^{-1}, and **H-Yb** shows a slight bathochromic shift (Fig. 1a). Upon excitation at the Soret or Q band, the Yb^{3+} complexes present intense luminescence at *ca.* 900–1100 nm, derived from the characteristic $^2F_{5/2} \rightarrow {}^2F_{7/2}$ transition of Yb^{3+}. Interestingly, **F-Yb** displays distinct pH-sensitive fluorescence from pH 9.0 to 5.0 in aqueous solution, and shows a 7-fold enhanced Yb^{3+} emission (Fig. 1b). As controls, **H-Yb** and **F-Yb-1** showed negligible pH sensitive emission but had similar pK_a values (*ca.* 6.6, Fig. 1c) and the emission of the methyl ester compound **F-L-Yb** remained constant at different pH values (Fig. S1†). Accordingly, the lifetime of **F-Yb** was also prolonged from *ca.* 13.4 to 135 μs. The obtained pK_a value was *ca.* 6.6, estimated either by the emission intensity or the lifetime. Thus, we hypothesized that the switched "on/off" NIR emission is related to the acid–base equilibrium of 4-carboxylate in the ligand,[39] which modulates the lowest triplet state of the ligand and the consequent energy transfer to the metal center.

To verify this, we chose **F-Gd** as the example and measured the phosphorescence of **F-Gd** to estimate the lowest triplet excited state upon the protonation/deprotonation of 4-carboxylate. When the carboxylates were protonated, **F-Gd** exhibited intense vibrationally structured emission bands at 700–900 nm (Fig. S2†). When deprotonated, no phosphorescence was observed. Moreover, the nanosecond transient absorption (Fig. S3†) showed that deprotonated **F-Gd** exhibits a much shorter lifetime (0.2 μs) and a smaller ΔOD compared to protonated **F-Gd** (1.6 μs), suggesting that the deprotonation of 4-carboxylate strongly quenches the triplet state of porphyrinate. In addition, TD-DFT calculations further support that deprotonation leads to photoinduced electron transfer (PET); while the protonation of carboxylate suppresses the PET process, this allows energy transfer from the lowest triplet state

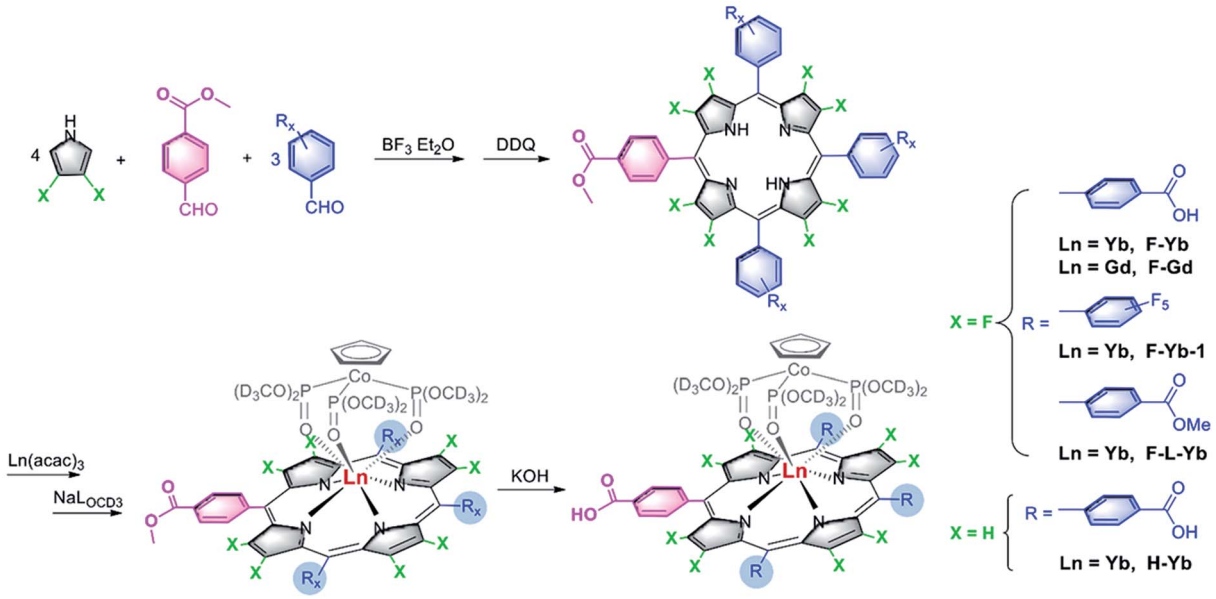

Scheme 1 Synthetic procedures of the lanthanide complexes studied in this work.

to the excited state of Yb^{3+} and switches on NIR luminescence, as shown in Fig. 2.

(2) pH 5.0–1.0. Decreasing the pH from 5.0 to 1.0 quenches the NIR emission (Fig. 3a). In a sharp contrast to luminescence intensity, we observed the lifetimes elongated from *ca.* 135 to 170 μs (Fig. 3a and S4†) and showed good reversibility (Fig. 3b). As **F-Yb** is highly acid-proof in the presence/absence of light (Fig. S5†), the emission change was not due to the decomposition but probably due to the aggregation of **F-Yb**. We assumed that the protonation of **F-Yb** lowers the solubility and tends to form **F-Yb** aggregates in acidic aqueous solutions.

Transmission electron microscopy (Fig. 3c) and dynamic light scattering (Fig. S6†) studies revealed that **F-Yb** aggregates in aqueous media and the mean diameters increase gradually from pH 5.0 (<5 nm) to 1.0 (*ca.* 200–300 nm). We tentatively correlated the decreasing fluorescence intensity to the "decreasing solubility" arising from the aggregation, as revealed by TEM and DLS studies. However, the lifetime is less affected by lumiphore concentration and the aggregation is likely to reduce the exposure of the Yb^{3+} complex to water (Fig. 3d), which has high energy O–H vibration and heavily quenches the NIR emission. Thus, we proposed that aggregation can enhance the rigidity of the complex and reduce the solvation effect on the NIR lifetimes.

Therefore, **F-Yb** displays a prolonged lifetime with decreasing pH from 9.0 to 1.0, showing that it is a wide-range pH τ probe. In addition, **F-Yb** displays almost a constant lifetime in aqueous solution with different viscosities (0–200 cP) and temperatures (0–50 °C), even in the presence of essential metal ions or oxidative-stress associated chemicals (glutathione, cysteine and H_2O_2) (Fig. S7†). It is worth noting that the aggregation elongated lifetime observed in this work is an interesting phenomenon for NIR Ln complexes, although intermolecular interaction is well-known to modulate the photophysical properties of fluorophores known as aggregation induced emission (AIE) and aggregation-caused quenching

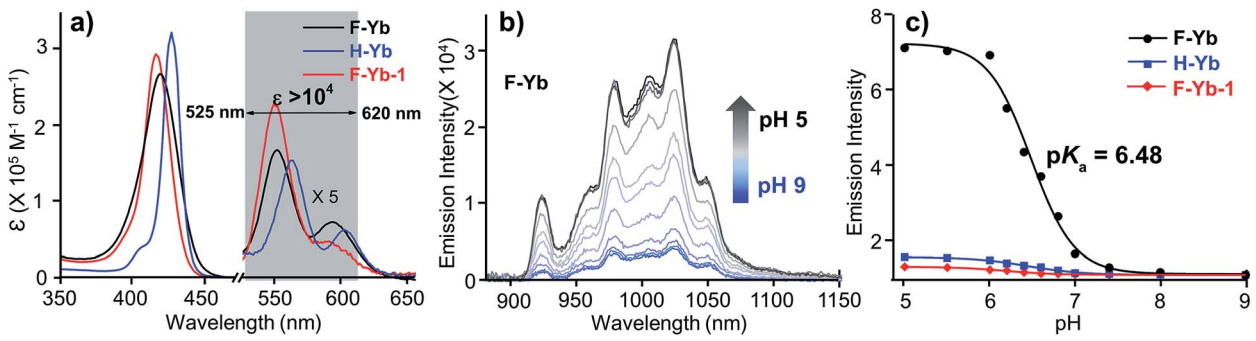

Fig. 1 (a) Absorption spectra of **F-Yb**, **H-Yb** and **F-Yb-1** in H_2O. (b) Fluorescence emission spectra of **F-Yb** in pH 5.0–9.0 PBS buffer. (c) The normalized emission intensity ratio according to the value at pH 9.0 *versus* the pH values in the pH range 5.0–9.0. All fluorescence emission spectra were obtained with 420 nm Xe lamp excitation and an 850 nm longpass emission filter.

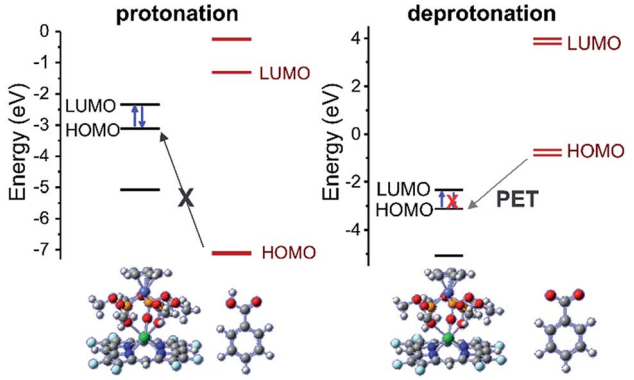

Fig. 2 Energies of the HOMOs and LUMOs of the centered porphyrin skeleton and the 4-carboxyphenyl group in the TD-DFT calculations under protonation/deprotonation.

(ACQ).[40] This might form a chemical basis to further design stimuli-responsive lanthanide τ probes.

Intracellular pH sensitivity

To study the pH-sensitivity of **F-Yb** in living cells, we performed NIR confocal imaging to monitor endogenous pH changes using chloroquine as an apoptosis inducer. Chloroquine is a well-known lysosomotropic agent that increases lysosomal pH by accumulating as a deprotonated weak base.[41] The intracellular NIR luminescence was initially found to localize in lysosomes (Fig. S8†). Upon the addition of 0.5 μM chloroquine, the NIR luminescence intensity decreased (*ca.* 60%), as shown in Fig. 4a. After 10 min, from the lysosomal luminescence intensity change, it is difficult to distinguish pH variation intracellularly. Interestingly, the parallel experiment using FLIM showed that the average lifetime of Yb^{3+} decreased from *ca.* 130 to 20 μs over a period of 30 min (Fig. 4b), indicating that the lysosomal pH increased from *ca.* 5.5 to 7.5 during the apoptosis process, similar to the previously reported results.[41] For the exogenous pH changes, we used the antibiotic nigericin as an H^+/K^+ ionophore to induce H^+ efflux.[42] By increasing the pH from 5.0 to 8.0 (Fig. S9†), **F-Yb** showed a shortened average lifetime from *ca.* 120 to 30 μs as well as decreased intracellular NIR luminescence (*ca.* 50%). We further examined the pH-sensitivity of **F-Yb** in HeLa spheroids with diameters of 100–200 μm using a nigericin inducer. As shown in Fig. 4c and d, the increasing pH from 5.0 to 8.0 lowers the NIR luminescence lifetime from *ca.* 120 to 35 μs. These results indicate that **F-Yb** provides not only higher sensitivity in terms of lifetime other than intensity but also quantitative readouts of both the endogenous and exogenous pH changes, suggesting its unique advantages as an NIR τ probe.

Prior to *in vivo* bio-imaging, we estimated the penetration depths with different modes: luminescence intensity and τ signals, by covering pork with a known thickness (0 and 3 mm) on the PBS buffer of **F-Yb** with various pH values. As shown in Fig. 5a, the EMICCD is triggered with a delay on the falling edge of the excitation laser, which ensures the exclusion of any extraneous excitation light. The fluorescence lifetime was then determined by a time-domain method and calculated from the slope of a plot of log $I(t)$ *versus* t ($I(t) = I_0\, e^{-t/\tau}$).[43] As expected, with an increase in penetration depth from 0 to 3 mm, the

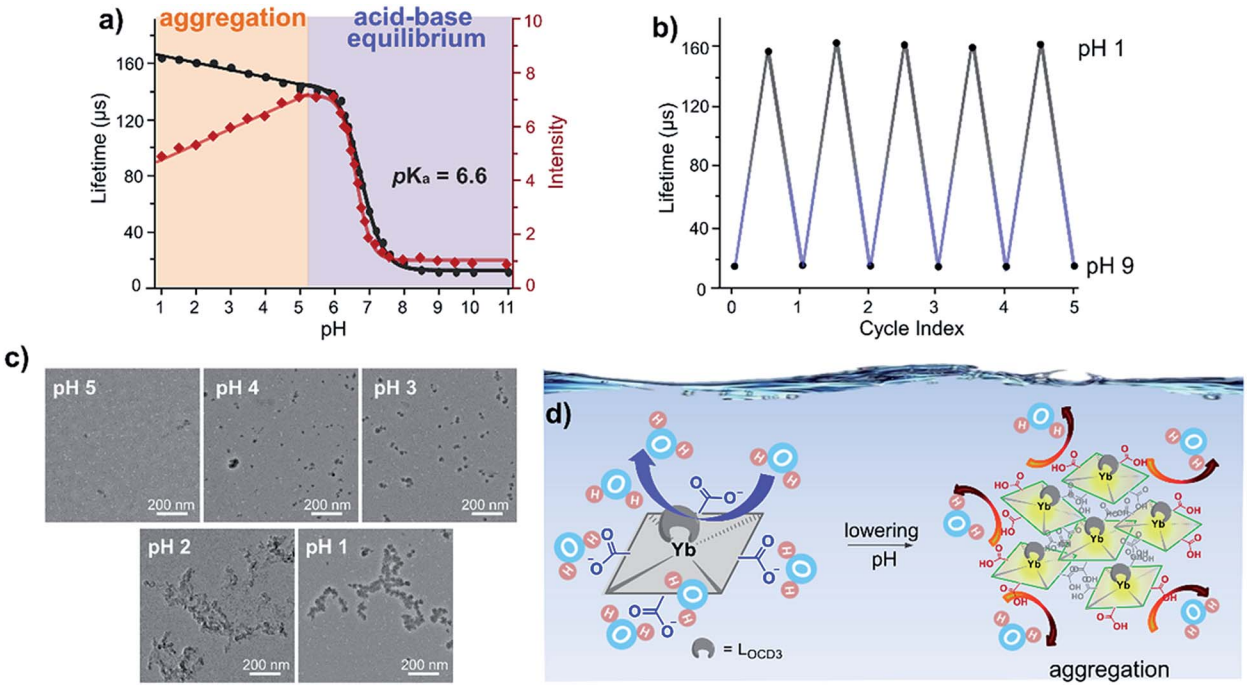

Fig. 3 (a) Lifetime values (blank) and the normalized fluorescence emission intensity ratio according to the value of **F-Yb** at pH 9.0 (red) *versus* the pH values in the pH range of 1.0–11.0. (b) Plot showing the reversible switching on/off of the lifetime of **F-Yb** between pH 1.0 and 9.0. (c) Transmission electron microscopy image and (d) schematic illustration of the aggregation of **F-Yb** at pH 1.0–5.0.

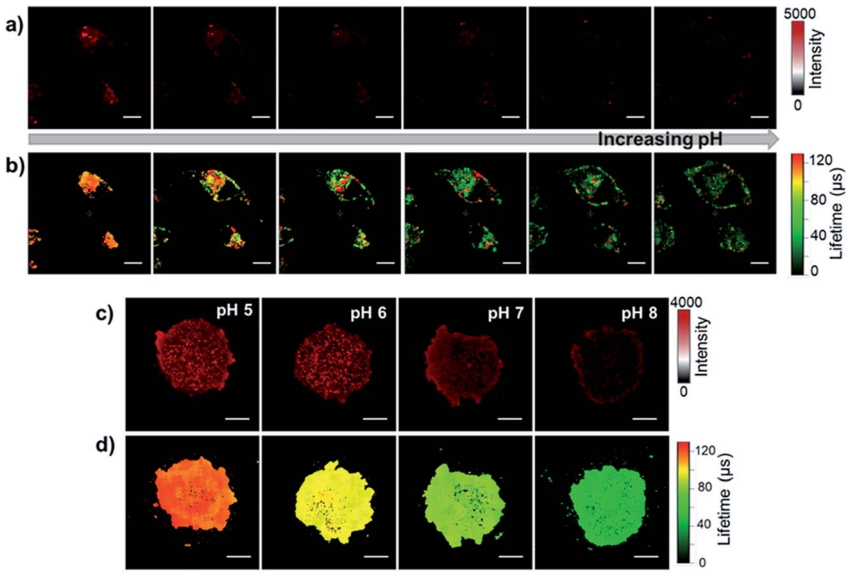

Fig. 4 (a) NIR confocal fluorescence images and (b) time-resolved fluorescence lifetime images of **F-Yb** (10 μM, 4 h) in HeLa cells stimulated with 0.5 μM chloroquine (λ_{ex}, 408 nm; λ_{em}, 935/170 nm bandpass; dwell time, 1 ms). Scale bar: 10 μm. (c) NIR confocal fluorescence images and (d) time-resolved fluorescence lifetime images of **F-Yb** (10 μM, 4 h) in 3D HeLa spheroids clamped at pH 5.0–8.0 in the presence of 10 μM nigericin (λ_{ex}, 408 nm; λ_{em}, 935/170 nm bandpass; dwell time, 1 ms). Scale bar: 40 μm.

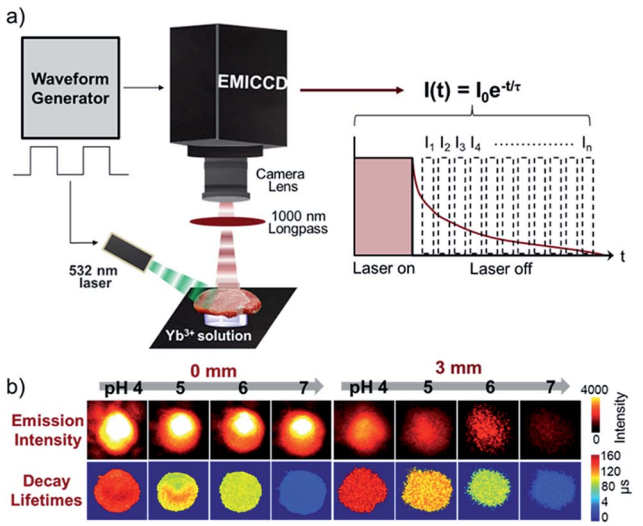

Fig. 5 (a) Schematic illustration of the penetration depth measurement of the emission and lifetime of **F-Yb**. The solution of **F-Yb** in a 96-well culture plate was covered with pork of a known thickness (0 and 3 mm) at various PBS buffer pH values (λ_{ex}, 532 nm; λ_{em}, 1000 nm longpass). (b) Emission intensity and lifetime of **F-Yb** in different pH values and penetration depths.

emission intensity significantly decreased upon excitation at 532 nm and varied in different pixels (Fig. 5b), indicating that it is not favorable to quantitatively measure pH values *in vivo*. In contrast, the lifetime of **F-Yb** remained constant at certain pH values, and was much less dependent on the penetration depth. By increasing the pH from 4.0 to 7.0, the lifetime decreased from *ca.* 150 to 30 μs. These results demonstrated the reliability and accuracy of **F-Yb** as an NIR pH τ probe. Although the excitation wavelength lies at the visible region, we herein demonstrated the effectiveness of pH detection under a penetration depth of *ca.* 3 mm using FLIM, and extending the excitation to deep red or the NIR region can be achieved by further modification of porphyrin structures.[29,44]

In vivo pH τ probe

Then, we applied the NIR τ probe **F-Yb** to *in vivo* pH detection. As the acidity (pH 1–3) of gastric fluid is usually lower than that of intestinal fluid (pH 6–7), the oral gavage experiments in nude mice were optional for monitoring the changes of both the fluorescence intensity and the lifetime of **F-Yb** *in vivo* from the stomach to the intestine (Fig. 6a). Mice were gavaged with 100 μL of 7 mg mL^{-1} **F-Yb** and anesthetized after the gavage. As shown in Fig. 6b, the NIR luminescence originally appeared in the stomach in the initial 10 minutes. With the emptying of **F-Yb** into the intestine, the fluorescence intensity in the stomach region gradually weakened, accompanied with an increase in fluorescence in the intestine. Until 170 min, the luminescence signal almost disappeared in the stomach and only existed in the intestine. By switching to FLIM mode, the **F-Yb** τ probe showed distinct lifetimes between the stomach (*ca.* 170 μs) and the intestine (*ca.* 110 μs), as shown in Fig. 6c. According to the pH curve shown in Fig. 3a, the pH values in the stomach and intestine were estimated as *ca.* 1.5 and *ca.* 6.0, respectively, which were consistent with the reported gastrointestinal pH values in mice.[45] Thus, using the NIR τ probe **F-Yb**, FLIM clearly provides the quantitative readouts to distinguish different organs according to the lifetimes under *in vivo* pH values.

To apply **F-Yb** as a non-invasive τ probe to monitor the dynamic pH variation in the metabolic process, we performed a fasting experiment which was a gastric related diagnostic and

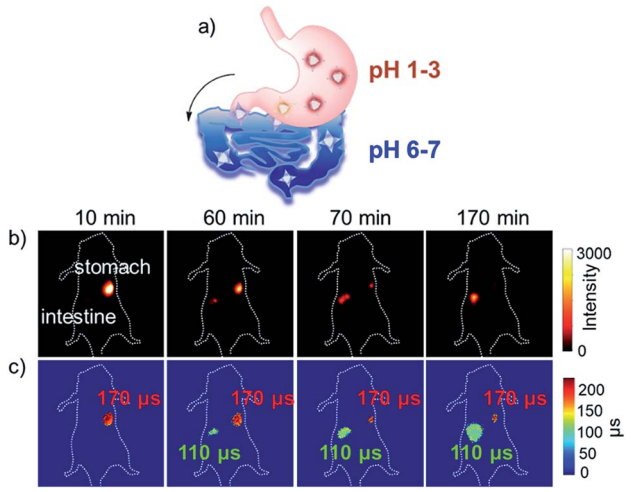

Fig. 6 (a) Schematic illustration of the metabolic process of **F-Yb** from the stomach to the intestine. (b) NIR fluorescence intensity imaging (exposure time, 25 ms) of the Yb^{3+} complex. (c) FLIM images (exposure time, 250 ms). λ_{ex}, 532 nm; λ_{em}, 1000 nm longpass.

the stomach pH was used as a key parameter (Fig. 7a).[45] Previously, as it was difficult to monitor stomach pH in the absence/presence of food, the fasting process was always performed by *ex vivo* experiments, where the mice were killed and the pH values were measured by a pH meter.[45] In this work, after fasting for 5 h, the mice were given a gavage of 100 μL **F-Yb** water solution (7 mg mL^{-1}) and the fitted average luminescence lifetime was calculated to be *ca.* 130 μs, indicating that the pH value increased to *ca.* 5.5 due to the inhibition of gastric acid secretion. Then, the mice were fed and the lifetime increased to *ca.* 170 μs, suggesting that the pH value was gradually recovered to *ca.* 1.5. However, as shown in Fig. 7b and c, fluorescence intensity imaging cannot distinguish the *in vivo* pH changes during the fasting experiments. Thus, compared to the *ex vivo* method, NIR FLIM mode using the NIR τ probe is suitable for non-invasive, real-time and quantitative measurements, enabling the visualization of the dynamic process that is related to *in vivo* pH changes.

The pH values in the gastrointestinal tract are crucial for clinical theranostics, as they affect the stability, solubility and potency of drugs.[46,47] To extend the application of the Yb^{3+} τ probe for *in vivo* NIR imaging-guided gastrointestinal therapeutics, we carried out a proof-of-concept study by giving the fed mouse 100 μL aqueous suspension containing hydrotalcite (2.6 mg) by gavage. Hydrotalcite chewable tablets have an obvious anti-acid effect[48] and the mouse dose was calculated based on the human dose and the specific surface area of both (Fig. 8a). 10 minutes after the gavage of the anti-acid medicine, the mice were fed with 100 μL **F-Yb** solution (7 mg mL^{-1}). As shown in Fig. 8b, the NIR luminescence intensity in the stomach decreased, accompanied with an increase in florescence in the intestine after 35 min. As expected, it is difficult to monitor the pH variation in the stomach after the treatment of hydrotalcite chewable tablets from the luminescence intensity alone. Using FLIM (Fig. 8c), the fluorescence lifetime of **F-Yb** in the stomach became much shorter after hydrotalcite treatment (*ca.* 120 μs) compared to that of the control group (*ca.* 170 μs), indicating the increased pH value. After 25 min, **F-Yb** gradually recovered to a lifetime of *ca.* 170 μs due to the hydrotalcite consumption and gastric acid secretion. Accordingly, we estimated the reversible stomach pH changes as *ca.* "1.5 (blank) → 6.5 (1 min) → 1.5 (35 min)" during the hydrotalcite treatment, referring to the pH calibration curve *in vitro* (Fig. 3a). Thus, the results demonstrate the ability of the **F-Yb** τ probe to monitor, real-time and reversibly, the pH changes, thus potentially aiding gastrointestinal treatment and the related drug design. As described above, a shortcoming of **F-Yb** is the visible excitation wavelength (500–600 nm), which limits the penetration length. In

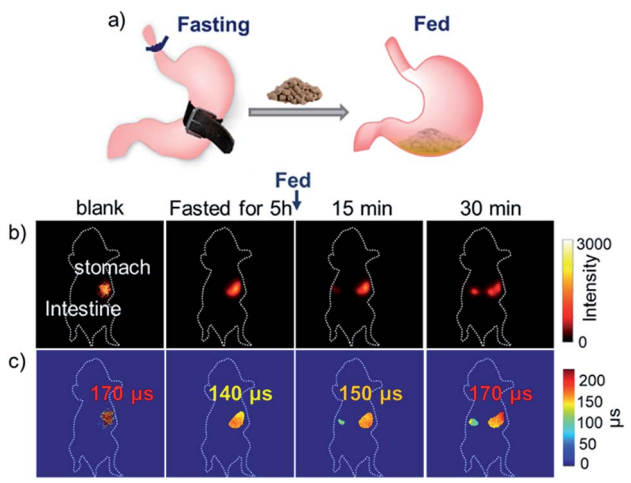

Fig. 7 (a) Schematic illustration of the fasting experiments with **F-Yb**. (b) NIR fluorescence intensity imaging (exposure time, 25 ms). The blue arrow at the top refers to the gavage of food. (c) FLIM images (exposure time, 250 ms). λ_{ex}, 532 nm; λ_{em}, 1000 nm longpass.

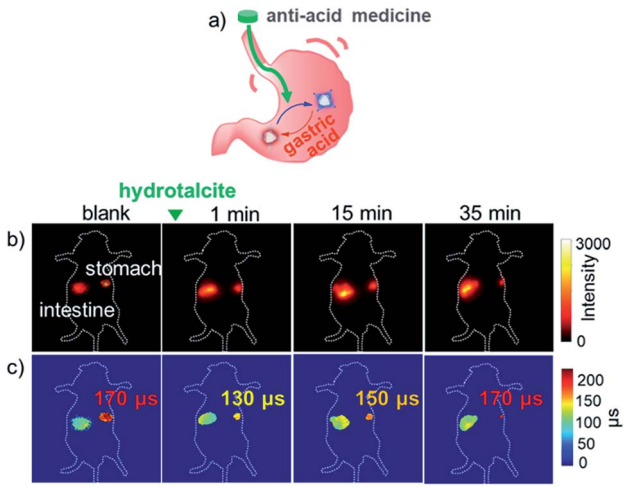

Fig. 8 (a) Schematic illustration of the monitoring of pH changes by **F-Yb** in the anti-acid process in the stomach. (b) NIR intensity fluorescence imaging (exposure time, 25 ms). The green triangle at the top indicates the gavage of hydrotalcite. (c) FLIM images (exposure time, 250 ms). λ_{ex}, 532 nm; λ_{em}, 1000 nm longpass.

this work, we demonstrated *in vivo* pH detection under a penetration depth of *ca.* 3 mm using FLIM.

Conclusions

Taken together, we report the design and synthesis of a wide-range NIR pH-responsive Yb τ probe for *in vivo* non-invasive diagnostics and therapeutics. Due to the long lifetime (μs scale) of lanthanide, the Yb^{3+} probe is able to quantitatively, dynamically and *in situ* monitor real-time pH changes in cells and *in vivo*, with deep penetration, good reversibility and high spatiotemporal resolution. The successful application of **F-Yb** in imaging-guided gastric related diagnostics and therapeutics demonstrates the superiority of NIR emissive Ln for *in vivo* molecular event visualization. This study paves the way for the design of lanthanide τ probes as "smart" materials in the NIR region.

Experimental section

Synthesis and characterization of the lanthanide complexes

For all synthesis and characterization details, please see the ESI.†

Photophysical properties

For the optical measurements, H_2O was obtained from a Milli-Q integral. UV-vis spectra were recorded on an Agilent 8453 UV-vis spectrometer equipped with an Agilent 89090A thermostat (±0.1 °C) at 25 °C. The emission, excitation spectra and lifetime were measured on an Edinburgh Analytical Instruments FLS980 lifetime and steady state spectrometer equipped with a 450 W Xe lamp, a 60 W microsecond flash lamp, a PMT R928 for the visible emission spectrum, and a HAMAMATSU R5509-73 PMT with a C9940-02 cooler for the NIR emission spectrum and luminescence lifetime measurements (850 nm longpass). Excitation and emission spectra were corrected for instrumental functions (including correction for the detector, gratings *etc.*). All luminescence decays were tail-fitted bi-exponentially with two components of *ca.* 170 and 15 μs as they gave small residuals and without deconvolution for the negligible instrumental reference function in the NIR region. The different pH solutions of **F-Yb** were prepared by diluting 2 mM concentrated **F-Yb** solution in Milli-Q water with Britton–Robinson buffer with different pH values. The final concentration was controlled at 10^{-6} M. The stabilities were determined by spiking **F-Yb** into KCl/HCl buffer (pH 1.5), and exposing it in a 1 mm-path-length cuvette with or without continuous 405 nm excitation (0.2 W cm^{-2}). The stability was determined by comparing the fluorescence intensity or lifetimes against the starting fluorescence intensity or lifetime values.

Transmission electron microscopy

3 μL 10^{-6} M of the well-dispersed **F-Yb** suspension in different pH values of Britton–Robinson buffer were dried on a copper grid. Then the copper grid was soaked in water for 12 h to dissolve the salt from the buffer and was then dried for 4 h before the test.

Cell cultures

HeLa cells were obtained from the Peking University Health Science Center. All of the HeLa cells were incubated in complete medium (Dulbecco's modified Eagle's Medium, supplemented with 10% fetal bovine serum (FBS) and 1% penicillin–streptomycin) at 37 °C in an atmosphere containing 5% CO_2. The dark cytotoxicity and photocytotoxicity of **F-Yb** towards the HeLa cells were measured by the standard Cell Counting Kit-8 (CCK-8) method and the complex showed low cytotoxicity (Fig. S10†). 3-D tumor spheroids were formed by seeding 5×10^3 to 1×10^4 HeLa cells per well in a volume of 200 μL per well of culture medium in 96-well plates coated with 1% agarose in complete DMEM medium. Tumor spheroids were allowed to grow for 2–3 days after the initial seeding and the growth was monitored by microscopy.

NIR confocal images

An ISS Alba5 FLIM/FFS confocal system (ISS Inc.) was used to acquire the confocal images. The system was attached a Nikon TE2000 inverted microscope, equipped with a Nikon 60X/1.2 NA water immersion objective lens. Both steady-state and time-resolved (lifetime) confocal images were acquired by the ISS VistaVision software and an ISS FastFLIM data acquisition unit. A 408 nm diode laser or YSL supercontinuum laser source (for excitation at the Q band) was used for the excitation of Yb^{3+} dye; the laser was operated in CW mode for steady-state imaging and was modulated on/off by a FastFLIM for lifetime imaging; the average power on the specimen plane was about 4 μW cm^{-2}. For lifetime imaging, the on/off repetition rate and the duty cycle were 1 kHz and 1%, respectively. A stock solution of the Yb^{3+} complex in H_2O was prepared at 2 mM. The solution was diluted to a final concentration of 10 μM by the complete growth medium. After incubation for 4 h, the cells were washed with PBS buffer twice before the confocal experiments. For the intracellular pH experiments induced by chloroquine, a stock solution of chloroquine was prepared at 1 mM, and the stock solution was added *in situ* to the PBS buffer to achieve a final concentration of 0.5 μM. For those induced by nigericin, the cells were incubated with a high K^+ buffer (30 mM NaCl, 120 mM KCl, 1 mM $CaCl_2$, 0.5 mM $MgSO_4$, 1 mM NaH_2PO_4, 5 mM glucose, 20 mM HEPES, and 20 mM NaOAc) at various pH values (5–8) in the presence of 10 μM of nigericin. Then the cells were incubated for 30 min at 37 °C before the fluorescence imaging measurements. The Yb^{3+} confocal images were acquired in Channel 1, using a Semrock 935/170 nm bandpass filter (EM1) and a single photon avalanche photodiode detector (SPAD) by Excelitas (model SPCM-AQRH-15, quantum efficiency >25% at 950 nm). For the co-localization studies, a 470 nm diode laser operated in CW mode was used for the excitation of LysoTracker Green. Stock solutions of LysoTracker Green DND-26 were prepared at 1 mM, and the stock solution was diluted to the working concentrations in the complete medium (Lyso Tracker: 75 nM). After incubation of the 10 μM Yb^{3+} complex for

4 h followed by 30 min incubation with the 75 nM solution of Lysotracker Green, the cells were washed with PBS buffer twice before the confocal experiments. The LysoTracker Green confocal images were collected in Channel 2, using a Semrock 530/43 nm bandpass filter (EM2) and a GaAsP photomultiplier tube detector by Hamamatsu (Model H7422p-40). A 405/470/561/685 nm multi-edge dichroic beamsplitter (D2) by Chroma was used to separate the two excitation wavelengths (samples and lysosome tracker) from the corresponding emission wavelengths. A 650 nm longpass dichroic beamsplitter (D3) by Chroma was used to separate the emission light between Channel 1 and Channel 2. A variable pinhole (VP) was used for each imaging channel and was set to 1 Airy Unit for the confocal imaging. All of the fluorescence images were processed and analyzed using ImageJ.

In vivo NIR imaging

Four-week-old node female mice were obtained from the Second Military Medical University (Shanghai, China) and were housed under standard environmental conditions. All animal procedures were performed in accordance with the Guidelines for Care and Use of Laboratory Animals of Fudan University and were approved by the Animal Ethics Committee of School of Pharmacy, Fudan University. Mice were randomly selected from cages for all of the experiments. NIR imaging was performed with a home-made imaging system. A waveform generator was used to modulate the frequency, duty cycle and initial phase of a 532 nm pulse laser. An emICCD (Princeton Instruments) and a 1000 nm longpass filter were used to collect NIR luminescence signals. To ensure the survival and health of the mice, the gavage dose of water solution (7 mg mL^{-1} **F-Yb**) or aqueous suspension (containing hydrotalcite) was 100 μL per mouse and the dose of anti-acid medicine was 2.6 mg per mouse, which was calculated based on the size and weight of the mouse. After gavage, the mice were anesthetized with chloral hydrate. The power density on the surface of the nude mouse was 100 mW cm^{-2}. The images of the luminescence signals were analyzed with Matlab.

Conflicts of interest

There are no conflicts to declare.

Acknowledgements

We acknowledge financial support from the National Key Basic Research Support Foundation of China (2015CB856301) and the National Scientific Foundation of China (Grants No. 21778002, 21571007, 21621061 and 21527801). We also thank Prof. Dayong Jin from the University of Technology Sydney (Australia) for the help in the setup of the imaging system.

Notes and references

1 J. D. Gray and M. Shiner, *Gut*, 1967, **8**, 574–581.
2 P. R. Hastings, J. J. Skillman, L. S. Bushnell and W. Silen, *N. Engl. J. Med*, 1978, **298**, 1041–1045.
3 I. M. Modlin, K. D. Lye and M. Kidd, *Cancer*, 2003, **97**, 934–959.
4 H. Du, M. Liu, X. Yang and G. Zhai, *Drug Discovery Today*, 2015, **20**, 1004–1011.
5 R. Wang, L. Zhou, W. Wang, X. Li and F. Zhang, *Nat. Commun.*, 2017, **8**, 14702.
6 P. E. Marik and A. Lorenzana, *Crit. Care Med.*, 1996, **24**, 1498–1500.
7 K. Arshak, E. Jafer, G. Lyons, D. Morris and O. Korostynska, *Microelectron. Int.*, 2004, **21**, 8–19.
8 S. Zhang, A. M. Bellinger, D. L. Glettig, R. Barman, Y. A. Lee, J. Zhu, C. Cleveland, V. A. Montgomery, L. Gu, L. D. Nash, D. J. Maitland, R. Langer and G. Traverso, *Nat. Mater.*, 2015, **14**, 1065–1071.
9 C. Caparello, I. Bravi, P. Cantu, A. Grigolon, A. Tenca, A. Mauro and R. Penagini, *Neurogastroenterol. Motil.*, 2012, **24**, 951.
10 S. Okuda, T. Saegusa and T. Itoh, *An Endoscopic Method to Investigate Gastric Acid Secretion*, Hitachi Printing, Tokyo, 1966.
11 H. J. Park, C. S. Lim, E. S. Kim, J. H. Han, T. H. Lee, H. J. Chun and B. R. Cho, *Angew. Chem., Int. Ed.*, 2012, **51**, 2673–2676.
12 G. Hong, A. L. Antaris and H. Dai, *Nat. Biomed. Eng.*, 2017, **1**, 0010.
13 S. He, J. Song, J. Qu and Z. Cheng, *Chem. Soc. Rev.*, 2018, **47**, 4258–4278.
14 M. Y. Berezin and S. Achilefu, *Chem. Rev.*, 2010, **110**, 2641–2684.
15 K. Y. Zhang, Q. Yu, H. Wei, S. Liu, Q. Zhao and W. Huang, *Chem. Rev.*, 2018, **118**, 1770–1839.
16 M. Dahan, T. Laurence, F. Pinaud, D. S. Chemla, A. P. Alivisatos, M. Sauer and S. Weiss, *Opt. Lett.*, 2001, **26**, 825–827.
17 C. Chen, P. Zhang, G. Gao, D. Gao, Y. Yang, H. Liu, Y. Wang, P. Gong and L. Cai, *Adv. Mater.*, 2014, **26**, 6313–6317.
18 Y. I. Park, K. T. Lee, Y. D. Suh and T. Hyeon, *Chem. Soc. Rev.*, 2015, **44**, 1302–1317.
19 Y. Fan, P. Wang, Y. Lu, R. Wang, L. Zhou, X. Zheng, X. Li, J. A. Piper and F. Zhang, *Nat. Nanotechnol.*, 2018, **13**, 941–946.
20 I. Martinić, S. V. Eliseeva and S. Petoud, *J. Lumin.*, 2017, **189**, 19–43.
21 Y. Li, X. Li, Z. Xue, M. Jiang, S. Zeng and J. Hao, *Biomaterials*, 2018, **169**, 35–44.
22 A. J. Amoroso and S. J. Pope, *Chem. Soc. Rev.*, 2015, **44**, 4723–4742.
23 Y. Yang, P. Wang, L. Lu, Y. Fan, C. Sun, L. Fan, C. Xu, A. M. El-Toni, M. Alhoshan and F. Zhang, *Anal. Chem.*, 2018, **90**, 7946–7952.
24 H. E. Rajapakse, N. Gahlaut, S. Mohandessi, D. Yu, J. R. Turner and L. W. Miller, *Proc. Natl. Acad. Sci. U. S. A.*, 2010, **107**, 13582–13587.

25 M. Delbianco, V. Sadovnikova, E. Bourrier, G. Mathis, L. Lamarque, J. M. Zwier and D. Parker, *Angew. Chem., Int. Ed.*, 2014, **53**, 10718–10722.
26 U. Cho, D. P. Riordan, P. Ciepla, K. S. Kocherlakota, J. K. Chen and P. B. Harbury, *Nat. Chem. Biol.*, 2018, **14**, 15–21.
27 Y. Lu, J. Lu, J. Zhao, J. Cusido, F. M. Raymo, J. Yuan, S. Yang, R. C. Leif, Y. Huo, J. A. Piper, J. Paul Robinson, E. M. Goldys and D. Jin, *Nat. Commun.*, 2014, **5**, 3741.
28 A. T. Bui, A. Grichine, A. Duperray, P. Lidon, F. Riobe, C. Andraud and O. Maury, *J. Am. Chem. Soc.*, 2017, **139**, 7693–7696.
29 T. Zhang, X. Zhu, C. C. Cheng, W. M. Kwok, H. L. Tam, J. Hao, D. W. Kwong, W. K. Wong and K. L. Wong, *J. Am. Chem. Soc.*, 2011, **133**, 20120–20122.
30 A. D'Aleo, A. Bourdolle, S. Brustlein, T. Fauquier, A. Grichine, A. Duperray, P. L. Baldeck, C. Andraud, S. Brasselet and O. Maury, *Angew. Chem., Int. Ed.*, 2012, **51**, 6622–6625.
31 A. Foucault-Collet, K. A. Gogick, K. A. White, S. Villette, A. Pallier, G. Collet, C. Kieda, T. Li, S. J. Geib, N. L. Rosi and S. Petoud, *Proc. Natl. Acad. Sci. U. S. A.*, 2013, **110**, 17199–17204.
32 I. Martinic, S. V. Eliseeva, T. N. Nguyen, V. L. Pecoraro and S. Petoud, *J. Am. Chem. Soc.*, 2017, **139**, 8388–8391.
33 S. Comby and J. C. G. Bünzli, *Lanthanide near-infrared luminescence in molecular probes and devices*, Elsevier, Amsterdam, 2007.
34 S. J. Bradberry, A. J. Savyasachi, M. Martinez-Calvo and T. Gunnlaugsson, *Coord. Chem. Rev.*, 2014, **273–274**, 226–241.
35 M. Sy, A. Nonat, N. Hildebrandt and L. J. Charbonniere, *Chem. Commun.*, 2016, **52**, 5080–5095.
36 J. Y. Hu, Y. Ning, Y. S. Meng, J. Zhang, Z. Y. Wu, S. Gao and J. L. Zhang, *Chem. Sci.*, 2017, **8**, 2702–2709.
37 Y. Ning, J. Tang, Y. W. Liu, J. Jing, Y. Sun and J. L. Zhang, *Chem. Sci.*, 2018, **9**, 3742–3753.
38 T. Zhang, R. F. Lan, C. F. Chan, G. L. Law, W. K. Wong and K. L. Wong, *Proc. Natl. Acad. Sci. U. S. A.*, 2014, **111**, E5492–E5497.
39 L. K. Truman, S. Comby and T. Gunnlaugsson, *Angew. Chem., Int. Ed.*, 2012, **51**, 9624–9627.
40 J. Mei, N. L. Leung, R. T. Kwok, J. W. Lam and B. Z. Tang, *Chem. Rev.*, 2015, **115**, 11718–11940.
41 B. Poole and S. Ohkuma, *J. Cell Biol.*, 1981, **90**, 665–669.
42 J. R. Casey, S. Grinstein and J. Orlowski, *Nat. Rev. Mol. Cell Biol.*, 2010, **11**, 50–61.
43 J. R. Lakowicz, *Principles of Fluorescence Spectroscopy*, Springer, 2006.
44 R. Xiong, D. Mara, J. Liu, R. Van Deun and K. E. Borbas, *J. Am. Chem. Soc.*, 2018, **140**, 10975–10979.
45 E. L. McConnell, A. W. Basit and S. Murdan, *J. Pharm. Pharmacol.*, 2008, **60**, 63–70.
46 L. S. Schanker, P. A. Shore, B. B. Brodie and C. M. Hogben, *J. Pharmacol. Exp. Ther.*, 1957, **120**, 528–539.
47 W. N. Charman, C. J. H. Porter, S. Mithani and J. B. Dressman, *J. Pharm. Sci.*, 1997, **86**, 269–282.
48 V. Rives, *Layered double hydroxides: present and future*, Nova Science Publishers, New York, 2001.